Geophysical Research Letters

RESEARCH LETTER
10.1029/2025GL120682

Key Points:

- The 2025 Kamchatka earthquake had the largest slip (~9 m) at 200–400 km SW of the epicenter at a shallow plate interface
- The tsunami heights and waveforms of the 2025 and 1952 earthquakes were very similar
- The 1952 Kamchatka earthquake had an overall size and slip distribution similar to the 2025 event, although the interval was only 73 years

Supporting Information:

Supporting Information may be found in the online version of this article.

Correspondence to:
K. Satake,
satake@ncu.edu.tw

Citation:
Fujii, Y., & Satake, K. (2026). The slip distributions of the 1952 and 2025 Kamchatka earthquakes from tsunami waveforms recorded around the Pacific Ocean. *Geophysical Research Letters*, *53*, e2025GL120682. https://doi.org/10.1029/2025GL120682

Received 14 NOV 2025
Accepted 27 MAR 2026

Author Contributions:
Conceptualization: Kenji Satake
Data curation: Yushiro Fujii
Formal analysis: Yushiro Fujii
Funding acquisition: Kenji Satake
Methodology: Kenji Satake
Project administration: Kenji Satake
Software: Yushiro Fujii
Supervision: Kenji Satake
Writing – original draft: Kenji Satake
Writing – review & editing: Yushiro Fujii

The Slip Distributions of the 1952 and 2025 Kamchatka Earthquakes From Tsunami Waveforms Recorded Around the Pacific Ocean

Yushiro Fujii[1] and Kenji Satake[2,3]

[1]International Institute of Seismology and Earthquake Engineering, Building Research Institute, Tsukuba, Japan, [2]Department of Earth Sciences, National Central University, Taoyuan, Taiwan, [3]Earthquake Research Institute, the University of Tokyo, Tokyo, Japan

Abstract The July 2025 Kamchatka earthquake (Mw 8.8) generated Pacific-wide tsunamis. Inversion of 40 DART bottom pressure records revealed a large (~9 m) slip at 200–400 km southwest of the epicenter. This model reproduces the local geodetic data, and is similar to other finite fault models based on teleseismic and geodetic data. Inversion of the tide gauge data also shows a similar slip distribution. In this region, a great megathrust earthquake ($M \sim 9$) occurred in 1952, and produced similar tsunami waveforms at tide gauge stations. We also made an inversion of the 1952 tide gauge data, considering clock correction at each station, the elasticity of the Earth and sea water, and the station corrections. The result shows that the 1952 slip distribution is similar to that of 2025, except for the depth of the largest slip and the northern slip where foreshock and aftershocks occurred in 2025.

Plain Language Summary The July 2025 Kamchatka earthquake (Mw 8.8) was the seventh-largest earthquake in the last century. This earthquake was somewhat unexpected, occurring only 73 years after a similar giant earthquake at the same location in 1952. Typically, such giant megathrust earthquakes recur at intervals of a few to several centuries. This study estimated the sizes and slip distributions of both the 1952 and 2025 earthquakes using state-of-the-art tsunami simulation methods while accounting for potential clock errors of the paper analog records of the 1952 tsunami. The overall sizes and the slip distributions of both earthquakes were generally similar, except for the depth of the largest slip and the 1952 slip north of the epicenter. Since the largest slip exceeded cumulative slip due to the plate motion, the locations of the largest slip may have been slightly different for the 1952 and 2025 earthquakes.

1. Introduction

A great earthquake (M 8.8) occurred off the Kamchatka peninsula on 29 July 2025 at 23:24:52.5 (UTC), or in the morning of July 30 in local time. According to USGS (United States Geological Survey), the epicenter is 52.4948° N, 160.2395°E and the depth is 35 km. The USGS (Yin et al., 2026) also provided a finite-source model (slip distribution on the fault; Figure S8a in Supporting Information S1) (https://earthquake.usgs.gov/earthquakes/eventpage/us6000qw60/finite-fault), that shows the large slip occurred 100–400 km southwest of the epicenter, while a large foreshock (M 7.4 on July 20) and aftershocks (M 7.4 on September 13 and M 7.8 on September 18) occurred near or north of the epicenter.

The occurrence of this earthquake is somewhat surprising because a great earthquake with a similar size (M 9.0) occurred in 1952 at a similar location. According to USGS, the origin time was November 4, 16:58:30 (UTC) and the hypocenter was 52.623°N, 159.779°E, 22 km. The moment magnitude was estimated from the free oscillation of the Earth (Kanamori, 1976). The 1952 earthquake generated a Pacific-wide tsunami. Johnson and Satake (1999) conducted a tsunami waveform inversion and estimated the slip distribution of the 1952 event. The largest slip was located at a deep part of the subducting plate interface. Based on near-field tsunami data, MacInnes et al. (2010) concluded that the high slip region might have been shallower.

The analysis of Johnson and Satake (1999) had some limitations from a modern perspective. First, the effects of elastic Earth and sea water for long-distance traveling tsunami (Watada et al., 2014), which is known to produce ~1% delay compared to linear long wave, were not considered. Second, the tsunami simulation grids were relatively coarse (5 and 1 min of the arc), limiting the accuracy of tsunami travel times and waveforms at tide gauge stations. Third, possible clock errors of the analog tide gauge records in the 1950s were not considered.

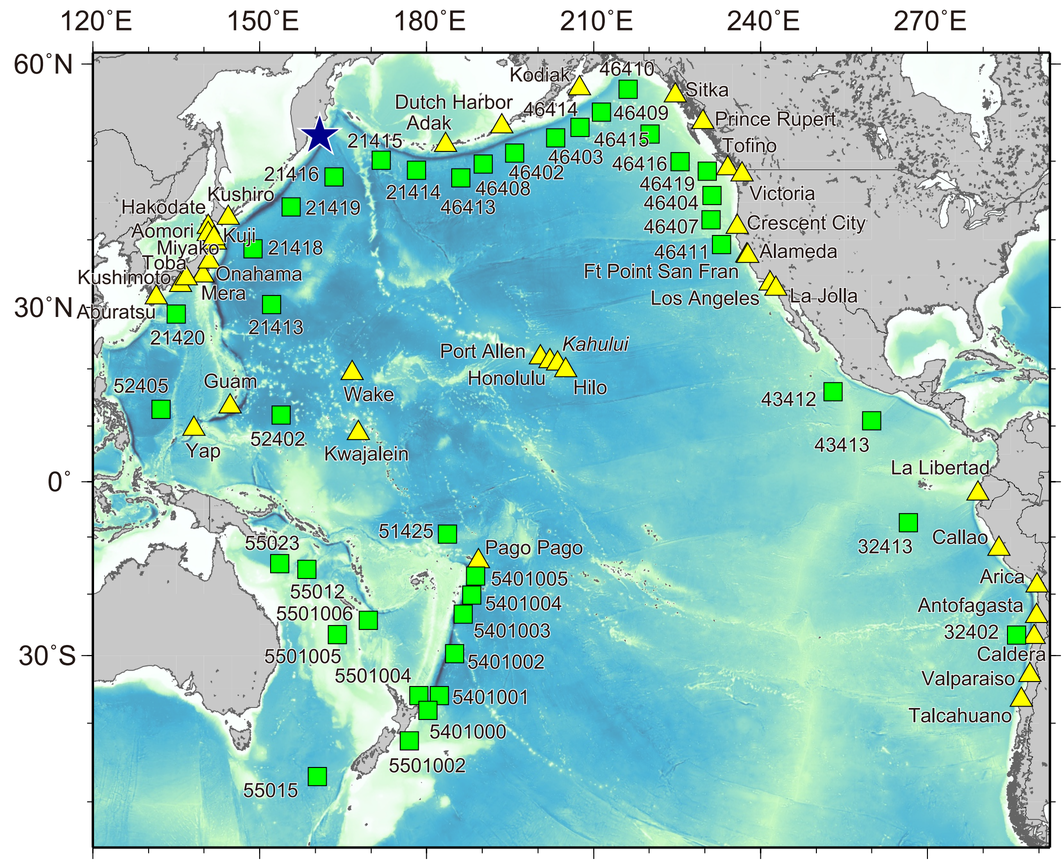

Figure 1. DART and tide gauge stations that recorded the 2025 and 1952 tsunamis. The green squares are DART stations that recorded the 2005 tsunami. The yellow triangles are the tide gauge stations that recorded both the 1952 and 2025 tsunamis. Data sources such as IOC, CMO, JMA, USCGS, and NCEI are listed in Table S1 in Supporting Information S1. The dark blue star is the epicenter of the 2025 earthquake. The 1952 epicenter is at a similar location (see Figure 3).

In this paper, we estimate the slip distributions of both the 2025 and 1952 earthquakes from tsunami waveforms, by considering the above limitations of the previous study. We first estimate the 2025 source using the DART (Deep-ocean Assessment and Reporting of Tsunamis) data, considering the elastic effects of the Earth and sea water. We then simulate the tsunami at tide gauge (TG) stations where both 1952 and 2025 tsunamis were recorded, and measure the time differences between the observed and simulated waveforms, that is, estimate the station corrections. We then make inversions of TG data as well as the joint inversion of DART and TG data. We further conduct inversion of the 1952 TG records, to estimate the slip distribution and clock error at each station, by considering the elastic effects and the station corrections.

2. Data

The 2025 tsunami was recorded on DART bottom pressure gauges and coastal tide gauges (TGs). We used tsunami waveforms recorded at 40 DART stations (Figure 1), downloaded from NOAA National Data Buoy Center (https://www.ndbc.noaa.gov/obs.shtml). Nearly half of them were recorded in the western Pacific Ocean, and the other half were in the eastern Pacific Ocean, providing good azimuthal coverage. In addition, we selected 37 TG stations that recorded both the 2025 and 1952 tsunamis. Among them, 10 were in Japan, 8 in the Pacific Ocean, 12 in North America, and 7 in South America (Figure 1). The TG data were downloaded from UNESCO IOC sea level station monitoring facility (https://www.ioc-sealevelmonitoring.org/). Several TG records in Japan were digitized from the Japan Meteorological Agency's press release (JMA, 2025). The tsunami waveforms are shown in Figure 2.

The 1952 tsunami was recorded on coastal TGs (with possible clock errors). We digitized the analog records from United States Coast and Geodetic Survey (USCGS, 1953), NOAA/NCEI, and Central Meteorological

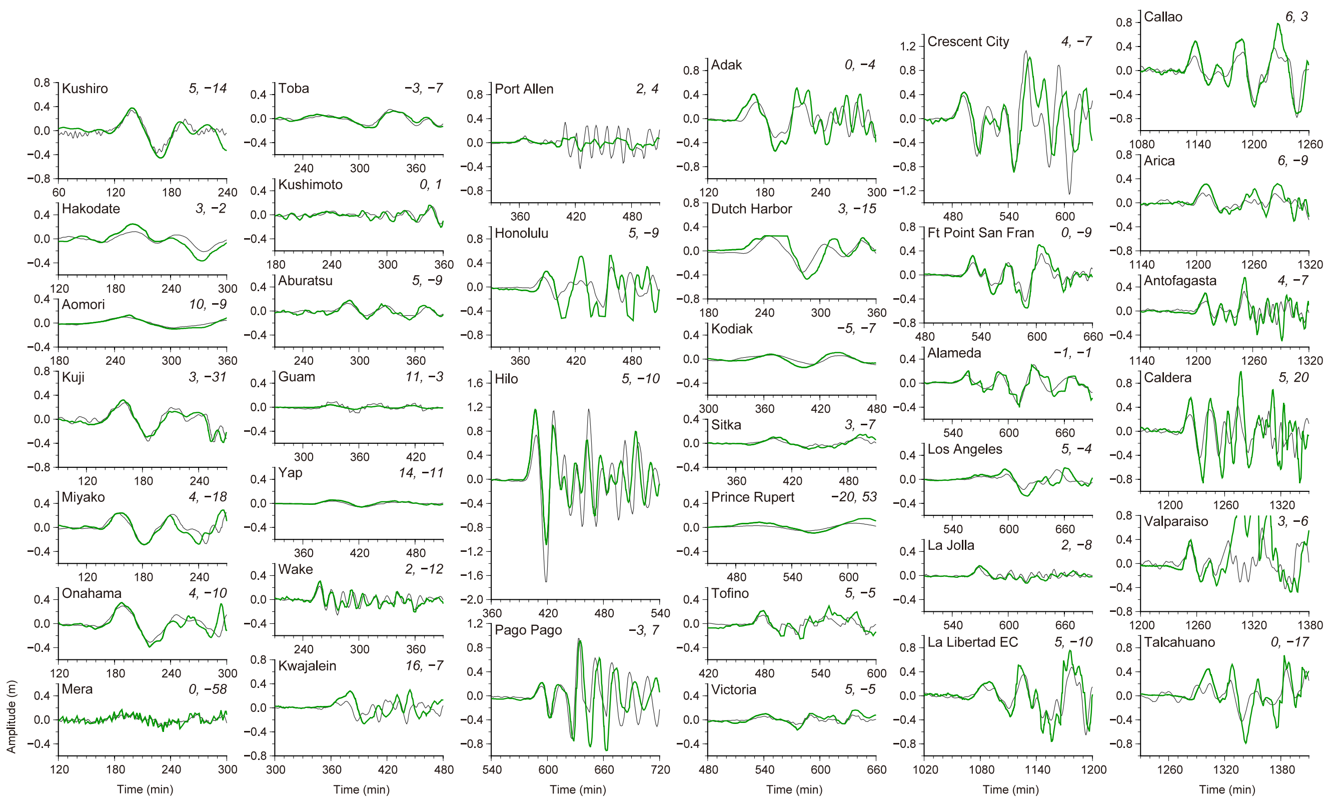

Figure 2. Comparison of the 2025 and 1952 observed tsunami waveforms. The black curves are the 2025 waveforms, and the green curves are the 1952 waveforms with clock corrections (Table S1 in Supporting Information S1) applied. The horizontal axis is time since the origin time of the earthquakes. The station corrections (min) for the calculated tsunami waveforms and the clock corrections (min) for the 1952 records, which are listed in Table S1 in Supporting Information S1, are indicated in the upper right corner of each station.

Organization (CMO, 1953) for the Japanese records. In the NCEI marigram database, digitized data were available at several stations; we downloaded and utilized them. They are also shown in Figure 2.

All the digital and digitized tsunami waveforms were resampled with a 1-min interval for analysis.

3. Method: Tsunami Waveform Inversion

To estimate the slip distribution on an earthquake fault, we placed 24 subfaults as shown in Figure 3 and Table 1. The subfault size is 100 km × 50 km. The strike is fixed at 218° and the slip angle at 90°. The top depth and the dip angles vary from 0 to 47 km and from 10° to 30° along with Slab 2.0 model (Hayes et al., 2018). We consider the rupture propagation with a constant rupture velocity of 2.5 km/s; the starting time of slip on each subfault is calculated from the epicentral distance divided by the rupture velocity. The rise time of slip on each subfault is fixed at 30 s. The seafloor displacement due to a unit amount of slip (1 m) is computed by the formulas of Okada (1985) with the effects of horizontal displacement and seafloor slope (Tanioka & Satake, 1996).

The tsunami Green's functions are computed based on the linear long wave theory (Fujii & Satake, 2024; Satake, 2015) in the region shown in Figure 1 (120°E–68°W and 55°S–61°N). The phase corrections for the elasticity of the Earth, compressibility of sea water, and gravitational potential variation (Watada et al., 2014), as well as the stratification of ocean layers (Ho et al., 2017), have been applied to the Green's functions, by employing the phase difference table of Ho et al. (2017). The 15 arc-sec bathymetry grid data from GEBCO 2024 (GEBCO Compilation Group, 2024) were resampled with a 24 arc-sec grid interval.

We first made a tsunami waveform inversion of the 2025 DART data. Because their locations are in the deep ocean, free from nonlinear and coastal topographical effects, and have a good azimuthal coverage, we believe that the DART inversion provides the most reliable results.

10.1029/2025GL120682

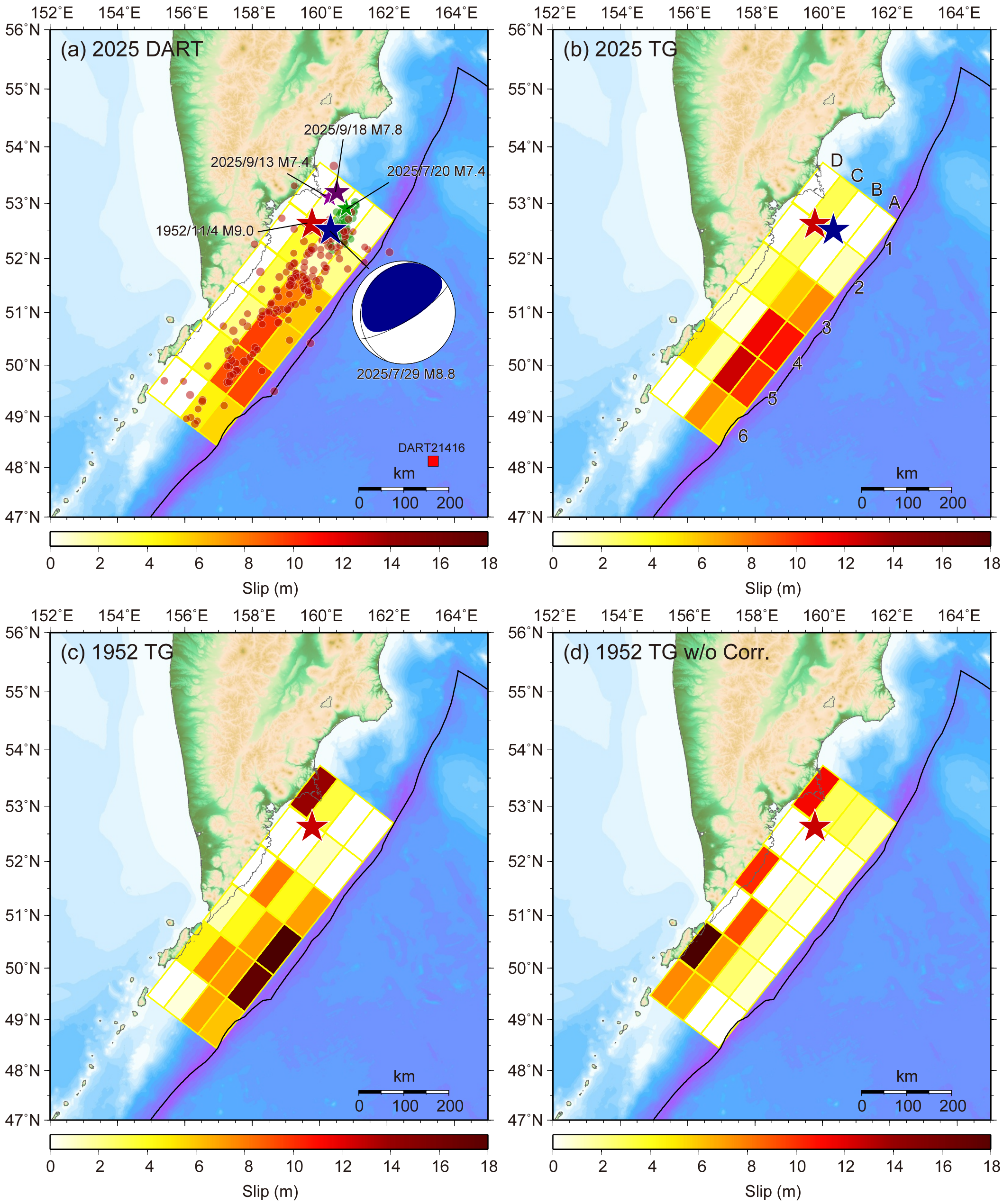

Figure 3. The slip distributions of the 2025 and 1952 Kamchatka earthquakes. (a) The 2025 slip from the inversion of DART. The focal mechanism solution of the 2025 mainshock is from the USGS W-phase Moment Tensor solution. The locations of the foreshock and aftershocks are also shown. Aftershocks (red circles) within one day and foreshocks (green circles) larger than M 5 by USGS are also shown. (b) The 2025 slip from the tide gauge (TG) inversion. Subfault numbers along strike and dip directions are shown. (c) The 1952 slip from the TG inversion considering the corrections of elasticity effects of the Earth and sea water (Watada et al., 2014). The red star indicates the epicenter determined by USGS. (d) The 1952 slip obtained without considering the elasticity effects.

We then computed the tsunami waveforms from the DART inversion, and compared them with the observed tide gauge (TG) data, to measure the timing shift at each station (Figure S1 in Supporting Information S1). These shifts are due to our numerical simulation with a rather coarse (24″ or ∼740 m) grid size, hence we considered them as station corrections of our numerical simulation (Table S1 in Supporting Information S1). We then made an inversion of the 2025 tsunami waveforms at TG stations after applying the station corrections. In addition, we

Table 1
Fault Parameters and Slips Inverted From Inversions

					Slip (m)			
#	Lat. (deg)	Lon. (deg)	Depth (km)	Dip (deg)	2025 DART	2025 TG	2025 DART and TG	1952 TG
1A	52.70000	162.20000	0.0	10	0.52	0.00	0.17	0.00
2A	51.99133	161.28632	0.0	10	2.08	1.21	1.83	0.00
3A	51.28265	160.38717	0.0	10	5.91	7.59	5.87	7.02
4A	50.57397	159.50196	0.0	10	5.96	10.76	6.51	18.40
5A	49.86530	158.63013	0.0	10	9.37	9.95	9.78	17.47
6A	49.15662	157.77116	0.0	10	5.56	5.51	6.35	6.04
1B	52.97263	161.62415	8.68	20	0.00	0.00	0.00	0.00
2B	52.26396	160.71963	8.68	20	1.14	0.00	0.58	1.12
3B	51.55528	159.82926	8.68	20	7.85	5.99	7.39	4.16
4B	50.84661	158.95249	8.68	20	9.61	11.46	10.51	7.06
5B	50.13793	158.08877	8.68	20	9.15	12.60	10.29	7.25
6B	49.42926	157.23759	8.68	20	4.60	7.52	5.52	6.88
1C	53.23278	161.07124	25.78	25	0.42	3.05	1.71	3.39
2C	52.52410	160.17559	25.78	25	3.69	2.28	3.45	0.00
3C	51.81543	159.29373	25.78	25	3.09	3.77	3.07	8.04
4C	51.10675	158.42513	25.78	25	2.20	0.42	1.86	4.19
5C	50.39808	157.56926	25.78	25	3.62	1.49	3.30	7.64
6C	49.68940	156.72564	25.78	25	0.00	0.00	0.00	0.64
1D	53.48368	160.53473	46.91	30	0.00	0.00	0.00	14.01
2D	52.77500	159.64778	46.91	30	0.00	0.00	0.00	0.00
3D	52.06633	158.77425	46.91	30	0.00	1.26	0.00	0.00
4D	51.35765	157.91367	46.91	30	0.00	0.99	0.00	1.43
5D	50.64898	157.06547	46.91	30	0.00	5.17	1.92	4.56
6D	49.94030	156.22924	46.91	30	0.00	0.00	0.00	0.00
				Mo (Nm)	1.87×10^{22}	2.28×10^{22}	2.00×10^{22}	2.98×10^{22}
				Mw	8.8	8.8	8.8	8.9

#: Subfault number. Lat., Lon., and Depth: Location and the top depth of the eastmost corners. Rigidity of 50 GP is assumed.

made a joint inversion of the DART and TG data, with a relative weight of 2.9:1, judging from the L2-norm of each data set.

The 1952 tsunami data may contain possible errors of clocks attached to tide gauges as well as timing errors in printing and digitizing the analog data. We call them clock errors, and simultaneously estimate the slip distribution and the clock error at each station by the OTA (Optimal Time Alignment) method (Ho et al., 2019; Romano et al., 2016).

For a quantitative comparison of models, we use variance reduction (VR) of tsunami waveforms. The larger VR indicates the better reproductivity of the observed waveforms. To examine the resolution of the inversion and uncertainty of the solution, we conducted checkerboard tests (Figure S6 in Supporting Information S1) by adding random noise with a 20% of amplitude at each station.

4. Results

The slip distributions from the 2025 DART and tide gauge (TG) inversions are shown in Figures 3a and 3b, respectively, as well as in Table 1. The DART inversion shows large (>9 m) slip in three subfaults at distances of 200–400 km SW of the epicenter with a depth of 0–26 km (below seafloor). The average slip is 3.1 m, providing a

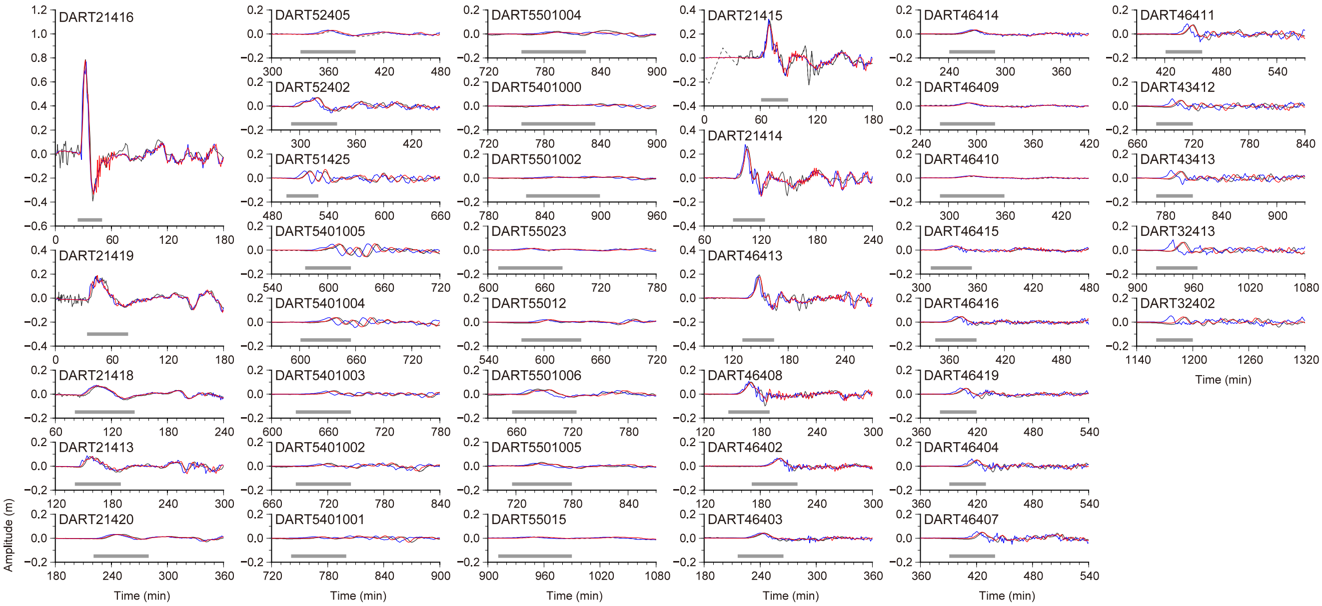

Figure 4. The 2025 tsunami waveforms at DART stations with synthetic waveforms from the DART inversion solution. The black curves are the observation, the red and blue curves are the synthetic waveforms with and without the corrections for the elasticity of the Earth and sea water (Ho et al., 2017; Watada et al., 2014). The dashed curves indicate the portion of 15-min sampling (e.g., clearly visible at station 21415 before tsunami arrival). The gray horizontal bars show the time windows used for the inversion.

total seismic moment of 1.87×10^{22} Nm (Mw 8.8), assuming the rigidity of 50 GPa. Comparison of the observed and simulated tsunami waveforms at DART stations (Figure 4) shows that they agree very well at all the stations, with variance reduction (VR) of 73%. Slight discrepancies in the tailing waves at nearby stations (21416, 21415, 21414, 46413) are due to dispersion effects, which are not included in our simulation. Figure 4 also shows simulated waveforms without considering the elastic effects. At far-field stations (travel times >420 min or 7 hr), the simulated waveforms arrive clearly earlier, because the elastic effects cause about 1% slower phase velocity, with a smaller VR of 52%.The 2025 TG inversion yields a similar result, but slightly larger average slip (3.8 m) and seismic moment (2.28×10^{22} Nm or Mw 8.8). The large slips occur at similar subfaults, but the amounts are larger (>10 m). Figure S2 in Supporting Information S1 shows the comparison of the observed and simulated tsunami waveforms at tide gauge stations. The simulated waveforms are very similar to the observed with a VR of 63%, including at Kahului where the largest tsunami amplitude was recorded (not used for the inversion).

The joint inversion of the DART and TG data (Figures S3 and S4 in Supporting Information S1) also shows a similar result, with an average slip of 3.3 m and a seismic moment of 2.0×10^{22} Nm or Mw 8.8. The VR is 69%, slightly lower than the DART inversion. The locations of the large slip are the same as the DART inversion (Figure 3a).

The inversion results of the tsunami (DART and TG) data can be compared with other geophysical data and models. Coseismic displacements in the Kamchatka peninsula computed from the tsunami inversion results reproduce the GNSS observations (Mikhailov et al., 2025) very well (Figure S7 in Supporting Information S1). The slip distributions from tsunami data (Figures 3a and 3b) are similar to the USGS finite-source model based on seismic data (Figure S8a in Supporting Information S1), as well as a fault model based on seismic and geodetic (InSAR) data by Liu et al. (2026) (Figure S8b in Supporting Information S1). The USGS model has much larger (>30 m) maximum slip, hence produces larger tsunami amplitude, while the fault model of Liu et al. (2026), which is similar to our model, reproduces the observed tsunami waveforms with a VR of 53% (Figure S9 in Supporting Information S1).

The 1952 slip distribution also has a large slip on subfaults at 200–400 km SW of the epicenter and the shallowest region (Figure 3c). The average slip (5 m) and the largest slip (18 m) are larger than those of the 2025 models (both DART and TG inversions). The seismic moment of 2.98×10^{22} Nm (Mw 8.9) is also larger than the 2025 earthquake. The simulated waveforms well reproduce the observed ones with a VR of 62% (Figure S5 in Supporting Information S1).

Two notable differences between the 2025 and 1952 slip distributions are the depth of the largest slip and the large slip north of the epicenter. The largest slip of the 2025 earthquake appears at subfaults 4B and 5B (the depth of 9–20 km beneath seafloor), while the largest slip of the 1952 earthquake appears at the shallowest subfaults (4A and 5A, depth 0–9 km). The northern slip (subfault 1D) appears only in 1952. This northern slip is required to explain the large and longer duration of the TG stations in the Aleutian Islands (Adak and Dutch Harbor), although the checkerboard test (Figure S6d in Supporting Information S1) shows that the resolution for the northwesternmost subfault is somewhat limited, that is, the slip amount may not be very reliable. The 2025 earthquake was preceded by a foreshock (M 7.4) and followed by aftershocks (M 7.4, M 7.8) to the north of the epicenter. No such large ($M \geq 7$) earthquake occurred before or after the 1952 earthquake in the source region. The lack of the northern slip may be due to the foreshock and aftershocks in 2025.

5. Discussion

The slip distribution of the 1952 Kamchatka earthquake, a large slip in the southwestern and shallow part of the source region, is quite different from that of Johnson and Satake (1999). The main reason is their lack of consideration of the elastic effects of the Earth and sea water, that were found by Watada et al. (2014). To confirm this, we made an inversion of the 1952 tsunami waveforms without making phase shifts for the Green's functions. The result (Figure 3d) shows large slips in the deeper part of the subduction zone, somewhat similar to that of Johnson and Satake (1999). However, the synthetic tsunami waveforms, with or without corrections of elastic effects, poorly reproduce the observed waveforms (Figure S5 and Table S2 in Supporting Information S1).

In the source region of the 2025 and 1952 earthquakes, giant earthquakes also occurred in 1841 and 1737. Unlike the 1952 and 2025 earthquakes, the 1841 and 1737 earthquakes did not leave tsunami waveforms on tide gauges, but the tsunami runup heights were recorded (NOAA/NCEI, Table S3 in Supporting Information S1). The tsunami heights in Hawaii were mostly 1–2 m, although the maximum of 4.6 m (1841) and 3.7 m (1952) were recorded. In general, the tsunami heights of these events were similar, and the tsunami magnitude (Mt) was about 9 (Abe, 1979). Gusev and Shumilina (2004) concluded that these earthquakes were of giant ($M \sim 9$) size, and estimated their recurrence intervals as 85–100 years (10–11.8 events in 1,000 years). Based on tsunami deposits, Pinegina et al. (2018, 2020) estimated that the recurrence of "typical" earthquakes as ∼130 years (30 events/4,000 years). They also estimated the recurrence of "full-length" events, with coastal subsidence, as ∼1,300 years (3 events/4,000 years). These intervals of giant ($M \sim 9$) earthquakes are shorter than those of other subduction zones (Satake & Atwater, 2007), and the 73 years between the 1952 and 2025 events may not be unusually short.

The convergence rate of the subducting Pacific Plate and the overlying North American plate is ∼8 cm/year, and the estimated backslip rate from the GPS analysis is up to nearly 8 cm/year, indicating a full coupling of the plate interface (Bürgmann et al., 2005). The interval between the last (1952) and the present (2025) earthquakes is only 73 years. If the strain was completely released in 1952, the accumulated slip would be 5.8 m, while the largest slip in the 2025 event was ∼9 m. As we have seen in the previous section, the largest slip appear at different subfaults between the 1952 and 2025 events, despite that the overall patterns are similar. The largest slip occurred at the shallowest subfault in 1952, but slightly deeper subfaults in 2025. Such a difference in slip depth also occurred along the Japan Trench (Satake et al., 2017). In 1896, the Meiji Sanriku tsunami earthquake ruptured with a large slip of ∼20 m at a depth of 3.5–7 km, where the slip of the 2011 Tohoku earthquake was 3–14 m. The largest slip of the Tohoku earthquake (20–36 m) occurred at shallower depth (0–3.5 km beneath seafloor), thus the shallowest slips were complementary. A similar complementary slip might have occurred in the Kamchatka subduction zone. During the 1952 Kamchatka earthquake, the accumulated strain had not been fully released, hence the slip amount in the 2025 earthquake may have been greater than the 73-year slip deficit.

6. Conclusions

The slip distributions of the 2025 and 1952 Kamchatka earthquakes were estimated from the tsunami waveforms recorded around the Pacific Ocean. The largest and average slips were ∼9 and 3.1 m for the 2025 event, and ∼18 and 5 m for the 1952 event. The seismic moments were 1.9×10^{22} Nm (Mw 8.8) for the 2025 earthquake and 3.0×10^{22} Nm (Mw 8.9) for the 1952 earthquake. The large slip appeared at 200–400 km southwest of the epicenter for both events, but the depth is slightly different. The largest slip appeared at a shallower depth in 1952 than in the 2025 event. This difference, or complementary slip, can explain the shorter interval than expected from backslip rate (∼8 m/century) estimated from GPS analysis (Bürgmann et al., 2005).

Conflict of Interest

The authors declare no conflicts of interest relevant to this study.

Availability Statement

The tsunami waveforms of the 2025 Kamchatka earthquake are available at the NOAA National Data Buoy Center (https://www.ndbc.noaa.gov/obs.shtml) and UNESCO IOC sea level station monitoring facility (https://www.ioc-sealevelmonitoring.org/). The 1952 tsunami waveforms are available from publications of United States Coast and Geodetic Survey (1953) and Central Meteorological Organization (1953), as well as at NCEI/WDS Global Historical Tsunami Database (National Geophysical Data Center, n.d.) (https://www.ncei.noaa.gov/products/natural-hazards/tsunamis-earthquakes-volcanoes/tsunamis).

Acknowledgments
We thank two anonymous reviewers, the associate editor, and the editor Daoyuan Sun for their constructive comments on the original manuscript. We also thank A. M. Konvisar for additional information about the GNSS location. All figures were generated using Generic Mapping Tools (Wessel & Smith, 1998). We thank Yoshie Fujii for her support in digitizing the tide gauge records and converting the tsunami waveform data. Kenji Satake is supported by Yushan Fellowship from Ministry of Education, Taiwan government.

References

Abe, K. (1979). Size of great earthquakes of 1837–1974 inferred from tsunami data. *Journal of Geophysical Research*, *84*(B4), 1561–1568. https://doi.org/10.1029/JB084iB04p01561
Bürgmann, R., Kogan, M. G., Steblov, G. M., Hilley, G., Levin, V. E., & Apel, E. (2005). Interseismic coupling and asperity distribution along the Kamchatka subduction zone. *Journal of Geophysical Research*, *110*(B7), B07405. https://doi.org/10.1029/2005JB003648
Central Meteorological Observatory. (1953). Report of the 1952 Kamchatka earthquake and tsunami. *Quarterly Journal of Seismology*, *18*(1), 1–48. (in Japanese). Retrieved from https://www.jma.go.jp/jma/kishou/books/kenshin/kenshin1.html
Fujii, Y., & Satake, K. (2024). Modeling the 2022 Tonga eruption tsunami recorded on ocean bottom pressure and tide gauges around the Pacific. *Pure and Applied Geophysics*, *181*(6), 1793–1809. https://doi.org/10.1007/s00024-024-03477-1
GEBCO Compilation Group. (2024). GEBCO 2024 grid. https://doi.org/10.5285/1c44ce99-0a0d-5f4f-e063-7086abc0ea0f
Gusev, A. A., & Shumilina, L. S. (2004). Recurrence of Kamchatka strong earthquakes on a scale of moment magnitudes. *Izvestiya - Physics of the Solid Earth*, *40*(3), 206–215. Retrieved from https://ns.emsd.ru/~gusev/2004/gusev_2004_recurrece.pdf
Hayes, G. P., Moore, G. L., Portner, D. E., Hearne, M., Flamme, H., Furtney, M., & Smoczyk, G. M. (2018). Slab2, a comprehensive subduction zone geometry model. *Science*, *362*(6410), 58–61. https://doi.org/10.1126/science.aat4723
Ho, T.-C., Satake, K., & Watada, S. (2017). Improved phase corrections for transoceanic tsunami data in spatial and temporal source estimation: Application to the 2011 Tohoku earthquake. *Journal of Geophysical Research*, *122*(12), 10155–10175. https://doi.org/10.1002/2017JB015070
Ho, T.-C., Satake, K., Watada, S., & Fujii, Y. (2019). Source estimate for the 1960 Chile earthquake from joint inversion of geodetic and transoceanic tsunami data. *Journal of Geophysical Research*, *124*(3), 2812–2828. https://doi.org/10.1029/2018JB016996
Japan Meteorological Agency. (2025). Regarding the earthquake near the Kamchatka Peninsula around 08:25 on July 30, 2025 (fourth report). (in Japanese). Retrieved from https://www.jma.go.jp/jma/press/2507/31a/202507311115.html
Johnson, J. M., & Satake, K. (1999). Asperity distribution of the 1952 great Kamchatka earthquake and its relation to future earthquake potential in Kamchatka. *Pure and Applied Geophysics*, *154*(3–4), 541–553. https://doi.org/10.1007/s000240050243
Kanamori, H. (1976). Re-examination of the Earth's free oscillations excited by the Kamchatka earthquake of November 4, 1952. *Physics of the Earth and Planetary Interiors*, *11*(3), 216–226. https://doi.org/10.1016/0031-9201(76)90066-2
Liu, C., Bai, Y., Lay, T., He, P., Wen, Y., Xiong, X., & Taymaz, T. (2026). Simple unilateral rupture of the great Mw 8.8 2025 Kamchatka earthquake. *Science*, *391*(6787), 812–817. https://doi.org/10.1126/science.aeb8232
MacInnes, B. T., Weiss, R., Bourgeois, J., & Pinegina, T. K. (2010). Slip distribution of the 1952 Kamchatka great earthquake based on near-field tsunami deposits and historical records. *Bulletin of the Seismological Society of America*, *100*(4), 1695–1709. https://doi.org/10.1785/0120090376
Mikhailov, V. O., Konvisar, A. M., Smirnov, V. B., Timoshkina, E. P., Titkov, N. N., Khairetdinov, S. A., & Chebrov, D. V. (2025). The rupture surface model of the July 29, 2025 Mw 8.8 Kamchatka earthquake based on satellite geodesy and interferometry data. *Doklady Earth Sciences*, *525*(2), 3. https://doi.org/10.1134/S1028334X25608752
National Geophysical Data Center. (n.d.). NCEI/WDS global historical tsunami database, 2100 BC to present [Dataset]. *NOAA National Centers for Environmental Information*. https://doi.org/10.7289/V5PN93H7
Okada, Y. (1985). Surface deformation due to shear and tensile faults in a half-space. *Bulletin of the Seismological Society of America*, *75*(4), 1135–1154. https://doi.org/10.1785/BSSA0750041135
Pinegina, T. K., Bazanova, L. I., Zelenin, E. A., Bourgeois, J., Kozhurin, A. I., Medvedev, I. P., & Vydrin, D. S. (2018). Holocene tsunamis in Avachinsky Bay, Kamchatka, Russia. *Pure and Applied Geophysics*, *175*(4), 1485–1506. https://doi.org/10.1007/s00024-018-1830-0
Pinegina, T. K., Bourgeois, J., Bazanova, L. I., Zelenin, E. A., Krasheninnikov, S. P., & Portnyagin, M. V. (2020). Coseismic coastal subsidence associated with unusually wide rupture of prehistoric earthquakes on the Kamchatka subduction zone: A record in buried erosional scarps and tsunami deposits. *Quaternary Science Reviews*, *233*, 106171. https://doi.org/10.1016/j.quascirev.2020.106171
Romano, F., Piatanesi, A., Lorito, S., Tolomei, C., Atzori, S., & Murphy, S. (2016). Optimal time alignment of tide-gauge tsunami waveforms in nonlinear inversions: Application to the 2015 Illapel (Chile) earthquake. *Geophysical Research Letters*, *43*(21), 11226–11235. https://doi.org/10.1002/2016GL071310
Satake, K. (2015). Tsunamis. In G. Schubert (Ed.), *Treatise on geophysics* (2nd ed.4, pp. 477–504). Elsevier. https://doi.org/10.1016/B978-0-444-53802-4.00086-5
Satake, K., & Atwater, B. F. (2007). Long-term perspectives on giant earthquakes and tsunamis at subduction zones. *Annual Review of Earth and Planetary Sciences*, *35*(1), 349–374. https://doi.org/10.1146/annurev.earth.35.031306.140302
Satake, K., Fujii, Y., & Yamaki, S. (2017). Different depths of near-trench slips of the 1896 Sanriku and 2011 Tohoku earthquakes. *Geoscience Letters*, *4*(1), 33. https://doi.org/10.1186/s40562-017-0099-y

Tanioka, Y., & Satake, K. (1996). Tsunami generation by horizontal displacement of ocean bottom. *Geophysical Research Letters*, *23*(8), 861–864. https://doi.org/10.1029/96GL00736

US Coast and Geodetic Survey (1953). *The tsunami of November 4,1952 as recorded at tide gauge stations* (Vol. 300, p. 62). U.S. Department of commerce, Special Publication.

Watada, S., Kusumoto, S., & Satake, K. (2014). Traveltime delay and initial phase reversal of distant tsunamis coupled with the self-gravitating elastic Earth. *Journal of Geophysical Research*, *119*(5), 4287–4310. https://doi.org/10.1002/2013JB010841

Wessel, P., & Smith, W. H. (1998). New, improved version of generic mapping tools released. *Eos, Transactions American Geophysical Union*, *79*(47), 579. https://doi.org/10.1029/98EO00426

Yin, H. Z., Allstadt, K., Barnhart, W. D., Clapp, S. A., Earle, P. S., Goldberg, D. E., et al. (2026). Rapid characterization of the 2025 8.8 Kamchatka, Russia earthquake. *The Seismic Record*, *6*(1), 1–12. https://doi.org/10.1785/0320250038